Science Advances

AAAS

advances.sciencemag.org/cgi/content/full/2/4/e1600001/DC1

Supplementary Materials for

Global marine pollutants inhibit P-glycoprotein: Environmental levels, inhibitory effects, and cocrystal structure

Sascha C. T. Nicklisch, Steven D. Rees, Aaron P. McGrath, Tufan Gökirmak, Lindsay T. Bonito, Lydia M. Vermeer, Cristina Cregger, Greg Loewen, Stuart Sandin, Geoffrey Chang, Amro Hamdoun

Published 15 April 2016, *Sci. Adv.* **2**, e1600001 (2016)
DOI: 10.1126/sciadv.1600001

This PDF file includes:

- fig. S1. ATPase activity of purified, recombinant mouse P-gp.
- fig. S2. Functional expression of mouse P-gp in yeast cells.
- fig. S3. Comparison of PBDE-100 interacting residues.
- fig. S4. Amino acid sequence alignment of human, mouse, zebrafish, and sea urchin P-gp.
- fig. S5. Levels of POPs in wild-caught yellowfin tuna.
- fig. S6. Individual POP congeners from the mixture inhibiting human P-gp.
- table S1. Data collection and refinement statistics of the mouse P-gp/PBDE-100 cocrystal structure.
- table S2. Metadata on yellowfin tuna specimens used in this study.
- table S3. Physical and chemical properties of the 10 POP inhibitors.
- References (*89*–*94*)

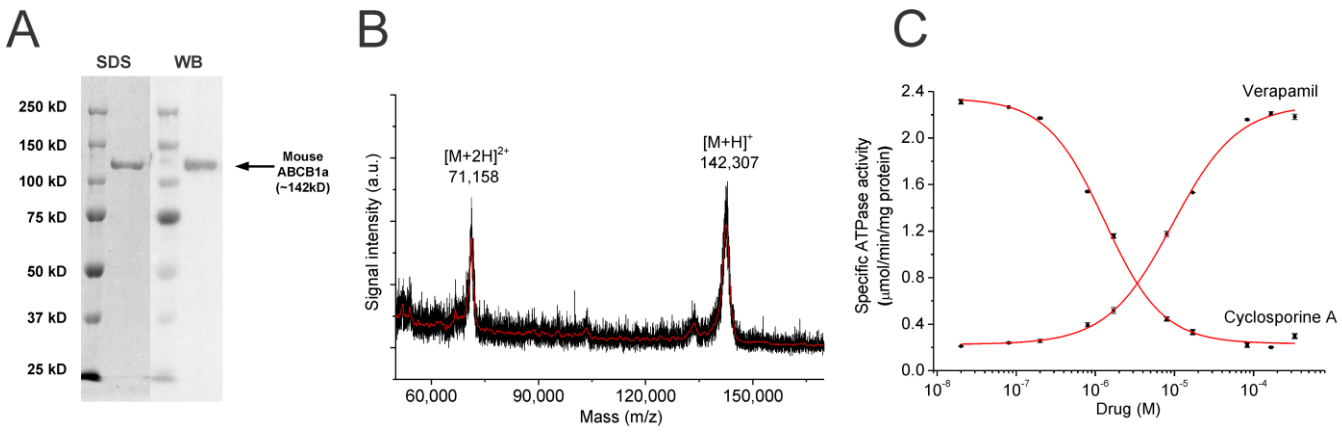

fig. S1. ATPase activity of purified, recombinant mouse P-gp. (**A**) 7.5% SDS-PAGE with Coomassie blue staining and an immunoblot (WB) of mouse P-gp fused to a C-terminal His_{10}-tag by anti-His antibody of purified P-gp protein. (**B**) MALDI TOF mass spectra of the purified mouse P-gp. Shown are two differently charged species of the protein (single and double charged ions). (**C**) ATPase activity of purified mouse P-gp using the malachite green method. ATPase activation and inhibition was determined with increasing concentrations of verapamil or cyclosporine A. Data points show specific ATPase activity from at least three independent experiments. Lines represent non-linear regression analysis of the data points with a Hill equation ($y = v_1 + (v_2 – v_1) * x^n / (k^n + x^n)$). R^2 values for the data fits were >0.99.

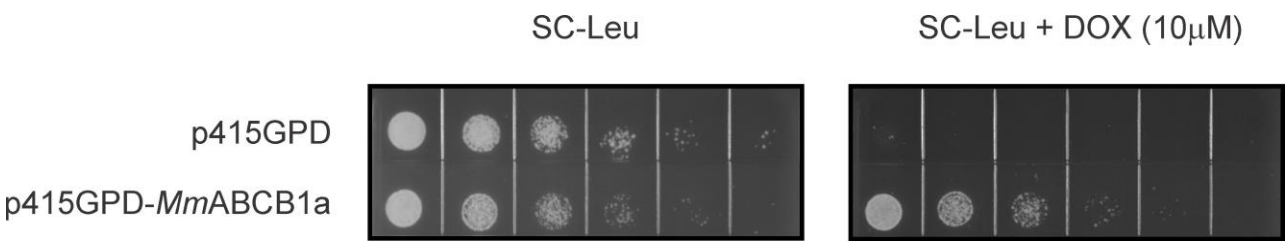

fig. S2. Functional expression of mouse P-gp in yeast cells. Hyper-sensitized MATα *S. cerevisiae* control strains and strains transformed with the p415GPD plasmid containing mouse P-gp were spotted in five-fold serial dilutions on SC-Leu (left panel) and SC-Leu + 10 μM doxorubicin (right panel) plates.

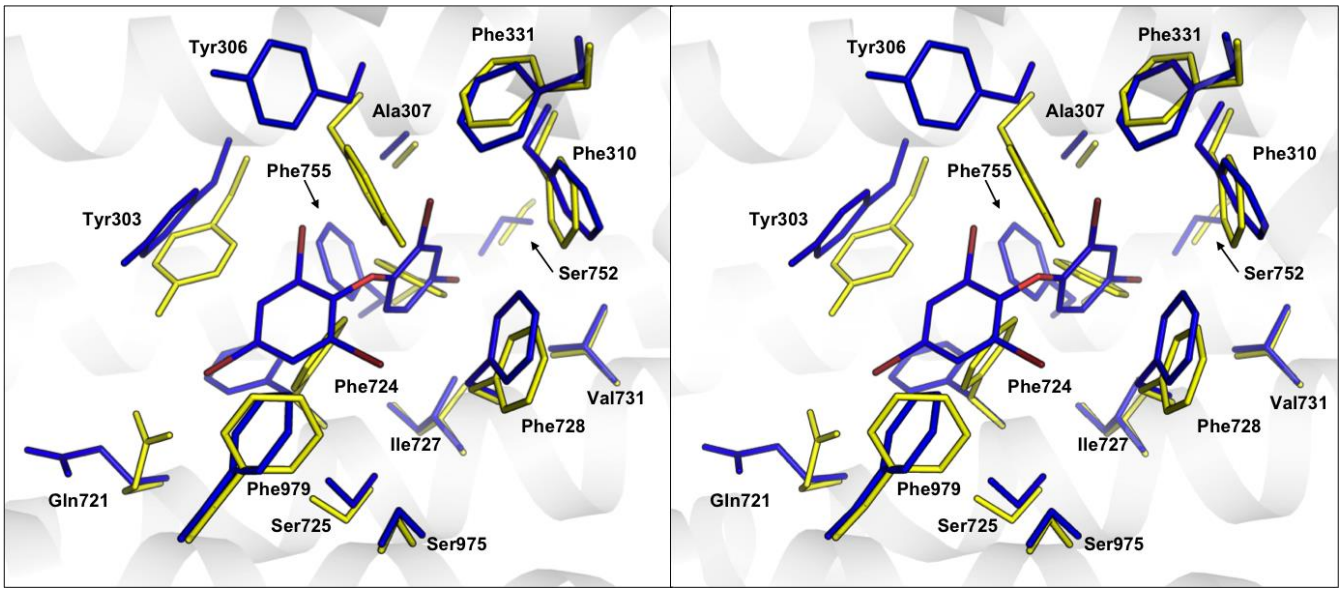

fig. S3. Comparison of PBDE-100 interacting residues. Alternative side-chain conformations adopted by P-gp ligand-interacting residues upon PBDE-100 binding are shown in blue compared to ligand-free P-gp (PDB code 4Q9H) shown in yellow.

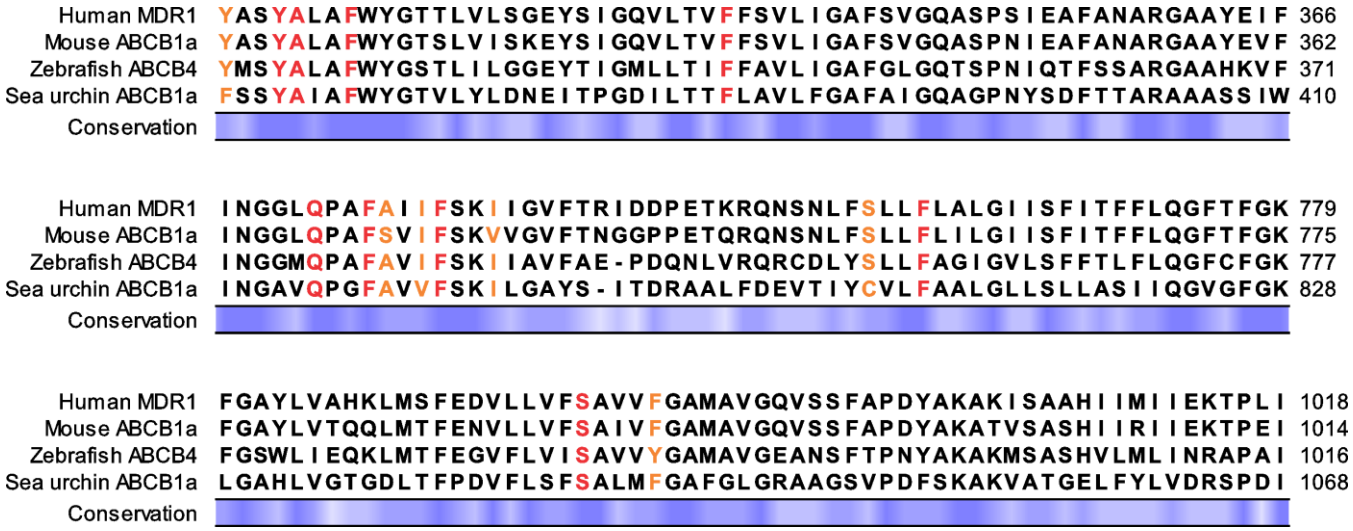

fig. S4. Amino acid sequence alignment of human, mouse, zebrafish, and sea urchin P-gp. PBDE-interacting residues are marked in red (conserved) and orange (non-conserved).

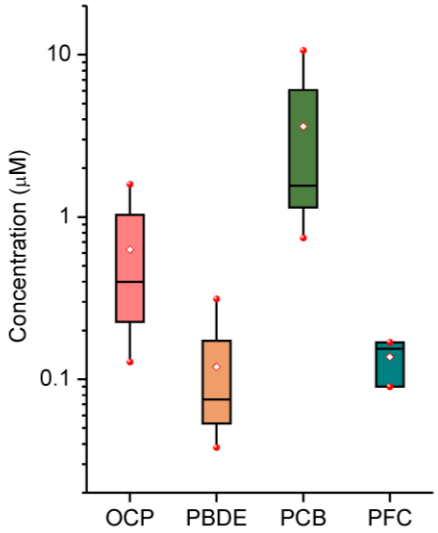

fig. S5. Levels of POPs in wild-caught yellowfin tuna. Box and whisker graphs represent the lipid normalized range of concentrations in micromolar of OCPs, PBDEs, PCBs, and PFC for eight fish caught in the Gulf of Mexico. The red-filled circles represent the minimum and maximum values. The white diamond represents the mean value. The horizontal line represents the 50th percentile, and the box represents the 25th and 75th percentiles.

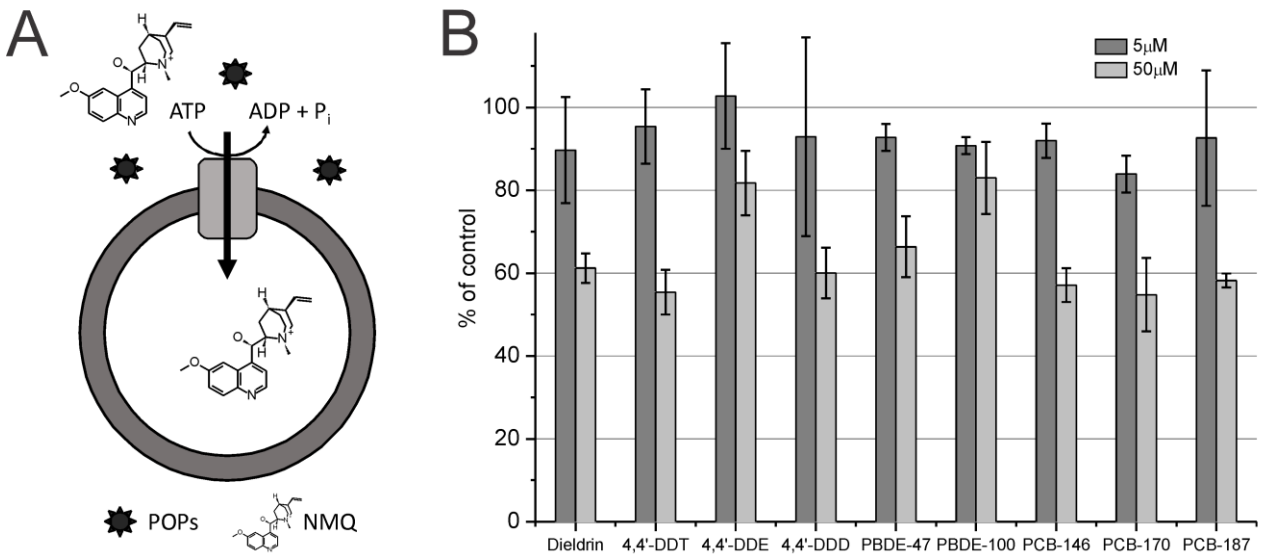

fig. S6. Individual POP congeners from the mixture inhibiting human P-gp. (**A**) Schematic illustration of the vesicular inhibition assay using human P-gp and NMQ as a substrate. (**B**) Inhibition of human P-gp by the 9 different congeners from the POP mixture. Bar graphs represent the average percentage of NMQ uptake ±S.D. relative to the control from 9 different experiments and at two different concentrations for each compound.

table S1. Data collection and refinement statistics of the mouse P-gp/PBDE-100 cocrystal structure.

	BDE100-Bound
PDB ID	
Data collection	
Wavelength	0.91929
Beamline	CLS-08ID
Space group	$P2_12_12_1$
Cell dimensions	
a, *b*, *c* (Å)	89.0, 138.2, 185.1
α, β, γ (°)	90, 90, 90
Resolution range (Å)	92.6-3.5 (3.7-3.5)
Number of crystals	1
R_{merge} (%)	7.7 (74.3)*
R_{pim}	5.5 (51.8)
Observed reflections	156577
Unique reflections	29261
Mean ((I/sd(I))	10.2 (2.2)
$CC_{1/2}$	0.998 (0.754)
Completeness (%)	99.3(99.9)
Redundancy	5.4 (5.4)
Refinement	
Resolution range (Å)	92.6-3.5 (3.6-3.5)
Reflections in working set	29204
Reflections in test set	1379
R_{work}/ R_{free}	26.3/28.2
R.m.s deviations	
Bond lengths (Å)	0.006
Bond angles (°)	0.988
<*B*> (Å^2), P-gp	139.17
<*B*> (Å^2), BDE100	178.16
Ramachandran statistics	
Outliers %	0
Favoured %	95.8
Rotomer Outliers %	0.6
Cβ Deviations	0

*Highest resolution shell is shown in parenthesis.

table S2. Metadata on yellowfin tuna specimens used in this study. Listed are the individual standard lengths and % of lipid from the fish caught in the Gulf of Mexico. The lipid-normalized levels of OCPs, PBDEs, PCBs, and PFCs as well as the sum of total POPs and the 10 P-gp inhibitors for each fish are shown in micromolar concentration. The fraction of the concentration of the ten inhibitors relative to the total POPs is listed in percent. ND = not detected.

Fish [#]	Standard length [cm]	Lipid [%]	ΣOCP [µM]	ΣPBDE [µM]	ΣPCB [µM]	ΣPFC [µM]	Total POPs [µM]	Inhibitors [µM]	Fraction [%]
1	114.3	0.36	1.59	0.26	10.10	ND	11.94	2.83	23.7
2	108.0	0.39	1.59	0.31	10.65	ND	12.56	2.88	22.9
3	86.4	1.29	0.48	0.09	2.04	0.09	2.69	0.59	22.1
4	99.1	2.33	0.47	0.08	1.53	0.15	2.23	0.44	19.7
5	99.1	1.19	0.33	0.07	1.53	ND	1.94	0.44	22.9
6	91.4	0.68	0.27	0.06	1.59	0.17	2.09	0.44	20.9
7	101.6	0.47	0.13	0.05	0.76	ND	0.93	0.22	23.6
8	99.1	0.72	0.18	0.04	0.74	ND	0.96	0.24	25.0

table S3. Physical and chemical properties of the 10 POP inhibitors. Listed are the molecular weights (MW) in g/mol, the octanol/water partition coefficients (Log K_{ow}), and the water solubilities in mg/L for each of the inhibitory compounds according to the respective ATSDR toxicological profile database (89-94).

POP congener	MW	Log K_{ow}	Water solubility at 25°C
Dieldrin	380.91	6.2	0.110
Endrin	380.91	5.34-5.6[a]	0.2
4,4' DDT (p,p' DDT)	354.49	6.91	0.025
4,4' DDE (p,p' DDE)	318.03	6.51	0.12
4,4' DDD (p,p' DDD)	320.05	6.02	0.090
BDE-47	485.79	6.81	0.015
BDE-100	564.69	7.24	0.04
PCB-146	360.88	6.7[b]	n.a.
PCB-170	395.32	7.1[b]	n.a.
PCB-187	395.32	7.1[b]	0.00047[c]

[a]Calculated values according to (91). [b]Values obtained from the Certificate of Analysis, Accustandard Inc. [c]Values according to (89).